Neighborhoods and Functionality in Metals (Supplementary Information)

M. Rajivmoorthy T. R. Wilson M. E. Eberhart

May 10, 2022

Contents

---

1 Comments on Computational Approach

Central to this investigation is the comparison of Bader atom energies with energies obtained with band methods. While conceptually undemanding, in practice these comparisons introduces sources of computational error. Band determined energies exploit variational methods while Bader atomic energies are calculated via the virial theorem [1, 2, 3]. In the latter case, even small errors in the calculated core electron energies can produce large total energy errors, which may be minimized using all electron methods and large basis sets. In turn, to facilitate comparison of Bader atom and band energies, to the extent possible, the same all electron basis sets and computational framework should be used for both calculations. The Amsterdam Modeling Suite provides the capabilities necessary to address many of these issues.

The suite utilizes the Amsterdam Density Functional (ADF) package [4, 5] to calculate the electronic structure of clusters, and BAND [6, 7, 5] to model extended crystalline systems. Both

codes use the same Slater-type-orbital (STO) basis functions, though some of the basis functions available to ADF are not fully supported by BAND, most consequential, the all electron quadruple zeta basis set including four polarization terms (QZ4P).

This became a factor when modeling the $4d$ transition metals where a QZ4P basis set was required to calculate Bader atom energies accurately. Presumably the large basis set was needed due to the greater number of radial nodes and hence more rapidly varying near nucleus charge density. Nonetheless, since BAND calculations could not be converged using the QZ4P basis set a source of computational error was introduced when comparing BAND determined formation energies with Bader atom energies. As a way of estimating the magnitude of this error, ADF was used to calculate single atom and large cluster total energies for all the $4d$ transition metal elements using both the triple zeta including two polarization terms (TZ2P) and QZ4P basis sets. In general, and not surprisingly, the single atom energies were lower for the larger basis set by about 10 eV. For the larger clusters, the total energy per atom was again lower using the QZ4P basis, but this time by about 10.6 eV per atom. Using the difference between the single atom and large cluster total energies as an approximation to the formation energy, the QZ4P basis set yields a more negative formation energy of approximately 0.6 eV per atom.

As a check on the accuracy of Bader atom energies we used the fact that over a Bader atom the integral of $\nabla^2\rho(r)$ should be identically zero [8, 9]. Deviations greater than 10^{-2} are deemed marginal and indicative of numerical error. We found that the integrated Laplacian of the charge density over the central Bader atom was sensitive to computational parameters. Best results were achieved with a high density Voronoi integration scheme (accint = 6), "very good" density fitting and an appropriate choice of basis set. Even so, in some circumstances the integral of $\nabla^2\rho(r)$ over the central Bader atom was slightly greater than 10^{-2}. However, at all times the same value over the central atom and the atoms of its first coordination shell were within acceptable limits. It is for this reason that we monitored the per atom energy of a "central cluster"—the central atom and its nearest neighbor coordination shell—as a function of changing boundary width. All calculations employed the generalized gradient approximation using the Perdew–Burke–Ernzerhof exchange-correlation functional (GGA PBE) [10]. Finally, the BAND calculations used a quadratic tetrahedron method for numerical integration over the Brillouin zone, sampling a minimum of 16 k points in the irreducible wedge.

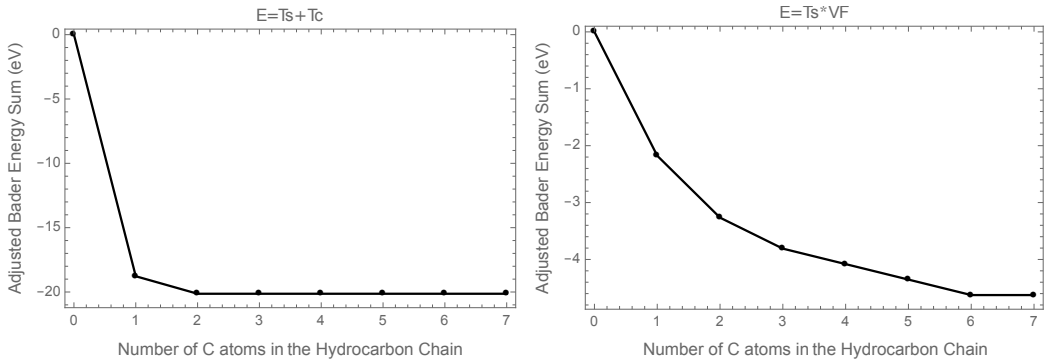

Figure 1: The energy for the aldehyde functional group is defined as the sum of Bader energies of C, H, and O atoms. This energy is plotted as a function of increasing C atoms in the hydrocarbon chain using the two representations described.

2 Determining the Bader Energy

The total energy over a volume bounded by zero flux surfaces is well-defined, and the Bader atom constitutes one such volume. It is common to calculate this energy using the virial theorem, *i.e.,* which for a system in mechanical equilibrium asserts that $E = -2T$ where E is the total energy and T is the kinetic energy. However, DFT methods do not compute a true kinetic energy, rather these methods compute the kinetic energy of the non-interacting electrons, T_{ni}. Still, though small, there is a contribution to the true kinetic energy from exchange and correlation and methods are available [3] that assert the ability to separate this contribution yielding a value denoted as T_c. The total kinetic energy can then be found as $T_c + T_{ni}$ and the total energy as $-2(T_c + T_{ni})$. This approach has been shown to work well in organic systems. Even so, in systems where there are forces acting on the nuclei (unrelaxed), there will be errors even if T_c were computed exactly.

As an alternative, one can calculate the virial factor, V_f by dividing the systems total energy by the noninteracting kinetic energy. The virial factor will be approximately, though not exactly, 2. By construction $\frac{-V_f}{T}$ gives the total system energy. V_f and the non-interacting kinetic energy of a Bader atoms can now be used to calculate a Bader atom total energy as $V_f\, T_{ni}$. This energy implicitly includes contributions to the total energy from exchange and correlation as well as being applicable in unrelaxed systems where there are forces acting on the nuclei. However, the approach assumes that the virial factor is uniform over the system, which we have found to be a reasonable assumption over nearly homogenous metallic clusters.

The convergence of the Bader energy determined for the aldehyde discussed in the main text

using these two quantities are summarized in Figure 1. Both show the rapid convergence of the functional group energy, though the virial factor approach converges more slowly and so represents a worst case scenario. Additionally, studies using T_c to compute total energy have not looked closely at metals; and some of our initial studies investigating Tc in metals showed unexplainable behavior. For these reasons, we have chosen the virial factor representation to define Bader energies for our studies of metallic systems.

3 Relativistic Effects

Relativistic effects will alter Bader energies. However, the codes used to compute Bader energies do not allow for relativistic corrections. Still, as our arguments are not based on the absolute energies but rather how these energies evolve as a perturbation is moved to greater distances, the absence of relativistic correction will not affect the form of this evolution. The basis for this argument is rooted in the fact that relativistic corrections in 4d transition metals are small and confined almost exclusively to core orbitals [11]. We expect that the relativistic correction if incorporated would simply add a constant to the exponentially decaying nearsightedness function.

4 Lattice data

The shell structure for the four lattice types (DC, BCC, HCP, and FCC) discussed in the main text is provided in Tables 1-4 and pictures of representative clusters shown in Figures 2-5.

Table 1: Face-centered cubic (FCC) shell structure. Row 1: Number of the coordination shell. Coordination shell zero is the central atom. Row 2: Number of atoms in coordination shell n. Row 3: Total number of atoms in the cluster of n coordination shells. (Hard sphere representations of some of these clusters are provided in the SI.) Row 4: Radius of the cluster, i.e. distance between the central atom and the atoms of the n^{th} shell in atomic diameters or equivalently nearest neighbor separations.

Coordination shell n	**0**	**1**	**2**	**3**	**4**	**5**	**6**	**7**	**8**	**9**	**10**
Number of n^{th} neighbors	1	12	6	24	12	24	8	48	6	48	24
Total atoms in cluster	1	13	19	43	55	79	87	135	141	189	213
Cluster radius	0	1	$\sqrt{2}$	$\sqrt{3}$	2	$\sqrt{5}$	$\sqrt{6}$	$\sqrt{7}$	$2\sqrt{2}$	3	$\sqrt{10}$

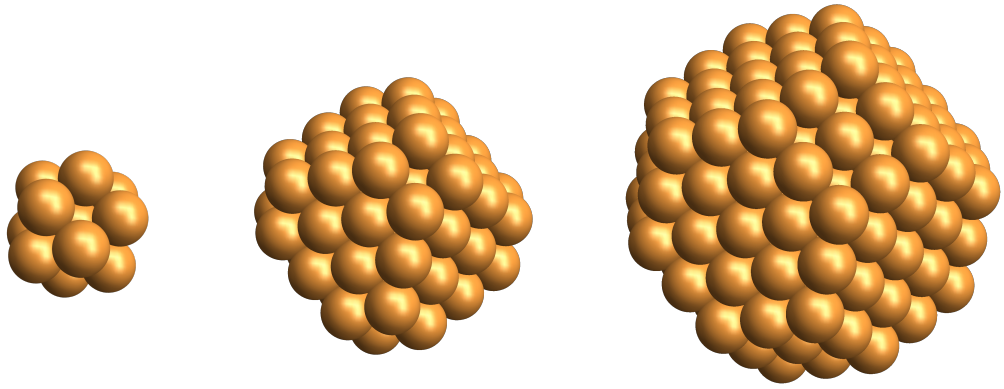

Figure 2: The FCC central 13-atom cluster (left), critical cluster consisting of 5 coordination shells (middle), and the largest cluster consisting of 10 coordination shells (right).

Table 2: Body-centered cubic (BCC) shell structure. Table layout is identical to that of Table 1.

Coordination shell n	**0**	**1**	**2**	**3**	**4**	**5**	**6**	**7**	**8**	**9**	**10**
Number of n^{th} neighbors	1	8	6	12	24	8	6	24	24	24	8
Total atoms in cluster	1	9	15	27	51	59	65	89	113	137	145
Cluster radius	0	1	$2\sqrt{\frac{1}{3}}$	$2\sqrt{\frac{2}{3}}$	$\sqrt{\frac{11}{3}}$	2	$4\sqrt{\frac{1}{3}}$	$\sqrt{\frac{19}{3}}$	$2\sqrt{\frac{5}{3}}$	$2\sqrt{2}$	3

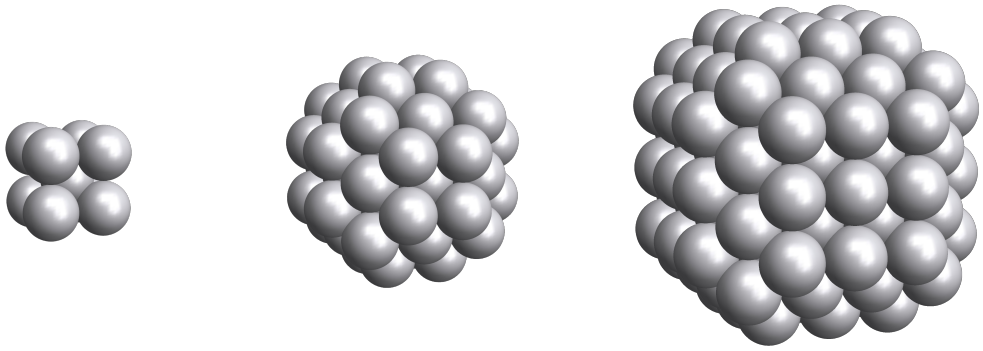

Figure 3: The BCC central 9-atom cluster (left), critical cluster consisting of 5 coordination shells (middle), and the largest cluster consisting of 10 coordination shells (right).

Table 3: Hexagonal close-packed (HCP) shell structure. Table layout is identical to that of Table 1.

Coordination shell n	**0**	**1**	**2**	**3**	**4**	**5**	**6**	**7**	**8**	**9**	**10**	**11**
Number of n^{th} neighbors	1	12	6	2	18	12	6	12	12	6	3	12
Total atoms in cluster	1	13	19	21	39	51	57	69	81	87	90	102
Cluster radius	0	1	$\sqrt{2}$	$2\sqrt{\frac{2}{3}}$	$\sqrt{3}$	$\sqrt{\frac{11}{3}}$	2	$\sqrt{5}$	$\sqrt{\frac{17}{3}}$	$\sqrt{6}$	$\sqrt{\frac{19}{3}}$	$2\sqrt{\frac{5}{3}}$

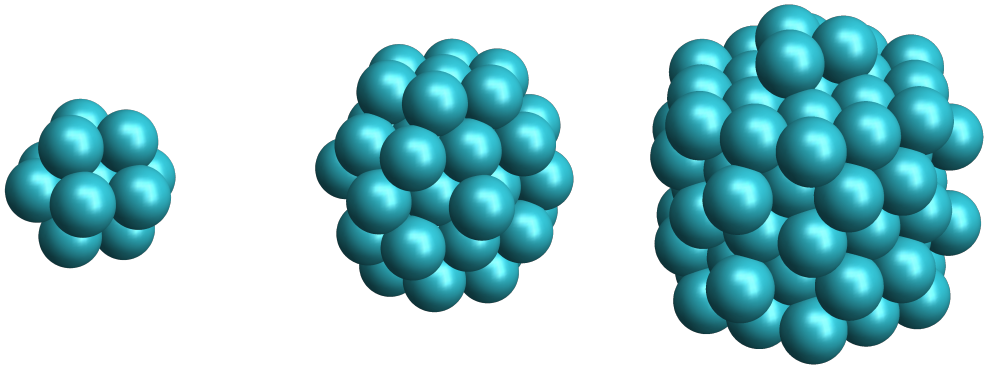

Figure 4: The HCP central 13-atom cluster (left), critical cluster consisting of 5 coordination shells (middle), and the largest cluster consisting of 11 coordination shells (right).

Table 4: Diamond cubic (DC) shell structure. Table layout is identical to that of Table 1.

Coordination shell n	**0**	**1**	**2**	**3**	**4**	**5**	**6**	**7**	**8**	**9**	**10**	**11**
Number of n^{th} neighbors	0	4	12	12	6	12	24	16	12	24	12	8
Total atoms in cluster	1	5	17	29	35	47	71	87	99	123	135	143
Cluster radius	0	1	$2\sqrt{\frac{2}{3}}$	$\sqrt{\frac{11}{3}}$	$4\sqrt{\frac{1}{3}}$	$\sqrt{\frac{19}{3}}$	$2\sqrt{2}$	3	$4\sqrt{\frac{2}{3}}$	$\sqrt{\frac{35}{3}}$	$\sqrt{\frac{43}{3}}$	4

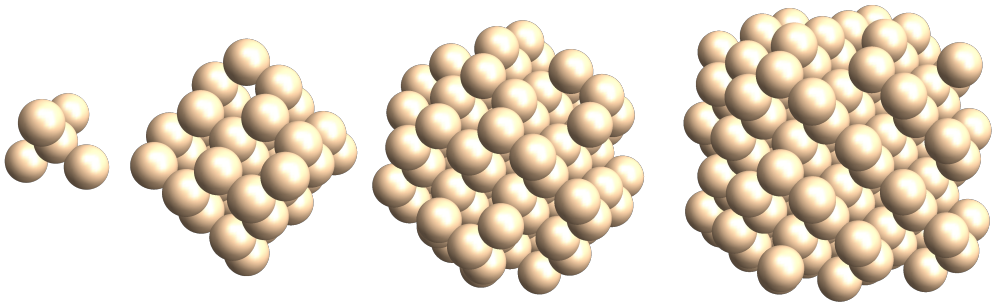

Figure 5: (from the left) The DC central 5-atom cluster, the 4-coordination cluster closing the central atom, the 7-coordination cluster closing the central cluster, and the largest cluster consisting of 11 coordination shells.

5 Element data

Data from which the graphs shown in the main text were constructed are provided in Tables 5-8.

Table 5: Perturbation energies ΔE of the (single) DC cluster investigated, reported in eV.

Element	**Diameter (Å)**	E_f	E_0	ΔE_1	ΔE_2	ΔE_3	ΔE_4	ΔE_5	ΔE_6	ΔE_7	ΔE_8	ΔE_9	ΔE_{11}
Si	2.352	-5.42	-7865.72	-3.05	-9.01	-5.66	-5.55	-6.09	-6.71	-6.67	-6.12	-5.91	-5.79

Table 6: Perturbation energies ΔE of FCC clusters, reported in eV.

Element	**Diameter (Å)**	E_f	E_0	ΔE_1	ΔE_2	ΔE_3	ΔE_4	ΔE_5	ΔE_6	ΔE_7	ΔE_9
Al	2.864	-3.78	-6587.00	-8.80	-5.86	-7.20	-	-4.65	-	-3.48	-4.08
Cu	2.553	-3.54	-44611.75	-3.64	-5.66	-3.83	-	-4.37	-	-3.56	-3.56
Rh	2.758	-6.78	-127504.31	-3.05	-4.00	-5.87	-	-6.32	-	-7.08	-
Pd	2.751	-3.99	-134362.32	-1.52	-2.22	-4.07	-	-4.71	-	-4.88	-
Ag	2.885	-3.71	-141429.58	-1.38	-2.13	-3.83	-	-3.90	-	-4.01	-

Table 7: Perturbation energies ΔE of BCC clusters, reported in eV.

Element	**Diameter (Å)**	E_f	E_0	ΔE_1	ΔE_2	ΔE_3	ΔE_4	ΔE_5	ΔE_6	ΔE_7	ΔE_8	ΔE_{10}
V	2.624	-8.36	-25665.42	-3.45	-4.35	-7.60	-8.99	-8.74	-8.82	-9.33	-9.04	-8.95
Nb	2.857	-10.22	-102139.80	-2.77	-4.06	-8.71	-9.39	-10.93	-11.02	-11.00	-11.06	-
Mo	2.725	-10.29	-108177.90	-1.57	-9.08	-8.29	-8.82	-10.16	-10.15	-11.51	-11.06	-

Table 8: Perturbation energies ΔE of HCP clusters, reported in eV.

Element	**Diameter (Å)**	E_f	E_0	ΔE_1	ΔE_2	ΔE_3	ΔE_4	ΔE_5	ΔE_6	ΔE_7	ΔE_9	ΔE_{11}
Tc	2.735	-11.52	-114414.78	-3.95	-4.87	-	-9.30	-10.70	-	-11.85	-12.06	-12.52
Ru	2.706	-9.79	-120855.98	-4.66	-5.07	-	-8.67	-9.78	-	-10.84	-11.10	-11.37

6 Dislocation Data

An edge dislocation dipole in Al was generated with the help of molecular dynamics simulations and corresponding clusters were generated from the structure.

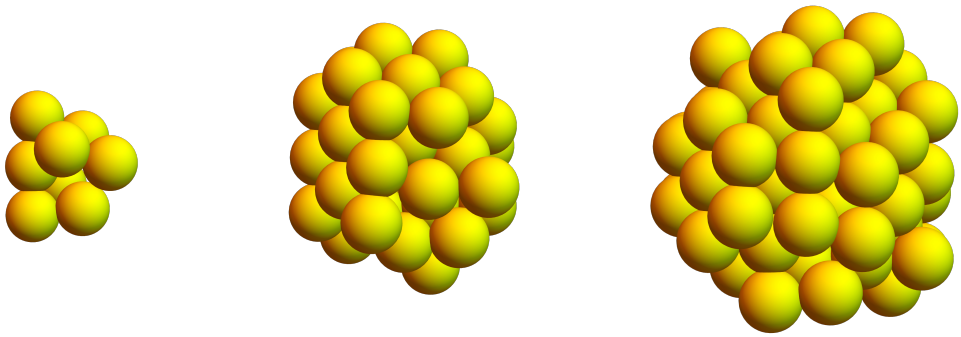

Figure 6: The central 9-atom Al dislcoation cluster (left), critical cluster consisting of 57 atoms (middle), and the largest cluster consisting of 88 atoms (right). These clusters are centered on the non-crystallographic hole corresponding to the dislocation.

Table 9: Perturbation energies $\boldsymbol{\Delta E}$ to the 9 atom first coordination shell surrounding the dislocation hole at the center in the Al dislcoation clusters Column 1: Number of atoms in the cluster. Coulmn 2: Cluster radii in units of Å. Coulmn 3: per atom energies of central cluster in eV – relative to isolated central cluster.

Number of atoms in cluster	**Cluster radii (Å)**	$\boldsymbol{\Delta E}$ **(eV/atom)**
9	3.190	0.00
14	3.943	-0.32
17	4.162	-0.45
23	4.453	-0.67
31	4.899	-0.75
38	5.397	-0.87
40	5.446	-0.87
50	5.813	-0.91
57	6.266	-0.80
64	6.452	-0.81
71	6.724	-0.70
88	7.311	-0.70

7 Grain boundary data

Grain boundaries are 2-dimensional defects that are present in real materials. They form the interface that separates the orientation in which atoms are stacked; and alter the microstructure, thus affecting performance. The data represented in graphical form in main text is provided in Tables 10-11 and pictures of important clusters in Figure 7.

Table 10: Perturbation energies $\boldsymbol{\Delta E}$ to the 14 atom first coordination shell surrounding the copper atom at the center in the $\Sigma 5$ grain boundary clusters Column 1: Number of atoms in the cluster. Coulmn 2: Cluster radii in units of Å. Coulmn 4: per atom energies of central cluster with Cu at center in eV – relative to isolated central cluster. Last row: Extrpolated values for ΔE_∞.

Number of atoms in cluster	**Cluster radii (Å)**	$\boldsymbol{\Delta E}$ **with Cu (eV/atom)**
15	2.906	0.00
23	4.280	0.14
31	4.638	-0.39
39	4.683	-0.55
47	4.812	-0.54
55	5.444	-0.54
63	5.725	-0.40
71	5.764	-0.10
77	5.893	0.28
83	6.528	0.38
93	6.817	0.41
97	6.873	0.44
∞	∞	0.45

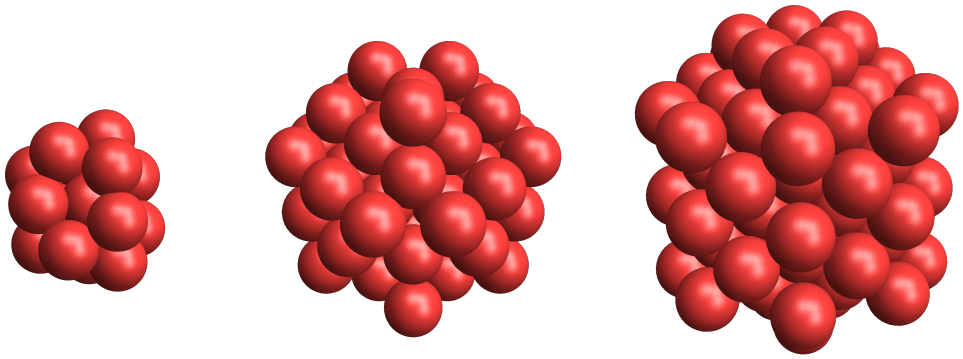

Figure 7: The grain boundary central 15-atom cluster (left), critical cluster consisting of 63 atoms (middle), and the largest cluster consisting of 97 atoms (right).

Table 11: Perturbation energies $\boldsymbol{\Delta E}$ to the 9 atom first coordination shell surrounding the grain boundary hole at the center in the Fe $\Sigma 5$ grain boundary clusters Column 1: Number of atoms in the cluster. Coulmn 2: Cluster radii in units of Å. Coulmn 4: per atom energies of central cluster in eV – relative to isolated central cluster.

Number of atoms in cluster	**Cluster radii (Å)**	$\boldsymbol{\Delta E}$ **(eV/atom)**
9	2.606	-0.26
11	3.436	-0.26
15	3.507	-0.24
23	3.968	-0.11
29	4.026	-0.17
33	4.240	-0.16
37	4.386	-0.16
41	4.551	-0.03
47	4.965	0.01
53	5.431	0.00

References

[1] J. C. Slater, *J. Chem. Phys.*, 1933, **1**, 687–691.

[2] K. Ruedenberg and M. W. Schmidt, *J. Phys. Chem. A*, 2009, **113**, 1954–1968.

[3] J. I. Rodríguez, P. W. Ayers, A. W. Götz and F. L. Castillo-Alvarado, *J. Chem. Phys.*, 2009, **131**, 021101.

[4] G. te Velde, F. M. Bickelhaupt, E. J. Baerends, C. Fonseca Guerra, S. J. A. van Gisbergen, J. G. Snijders and T. Ziegler, *J. Comput. Chem.*, 2001, **22**, 931–967.

[5] E. J. Baerends, T. Ziegler, A. J. Atkins, J. Autschbach, D. Bashford, A. Bérces, F. M. Bickelhaupt, C. Bo, P. M. Boerrigter, L. Cavallo, D. P. Chong, D. V. Chulhai, L. Deng, R. M. Dickson, J. M. Dieterich, D. E. Ellis, M. van Faassen, L. Fan, T. H. Fischer, C. F. Guerra, M. Franchini, A. Ghysels, A. Giammona, S. J. A. van Gisbergen, A. W. Götz, J. A. Groeneveld, O. V. Gritsenko, M. Grüning, S. Gusarov, F. E. Harris, P. van den Hoek, C. R. Jacob, H. Jacobsen, L. Jensen, J. W. Kaminski, G. van Kessel, F. Kootstra, A. Kovalenko, M. V. Krykunov, E. van Lenthe, D. A. McCormack, A. Michalak, M. Mitoraj, S. M. Morton, J. Neugebauer, V. P. Nicu, L. Noodleman, V. P. Osinga, S. Patchkovskii, M. Pavanello, C. A. Peeples, P. H. T. Philipsen, D. Post, C. C. Pye, W. Ravenek, J. I. Rodríguez, P. Ros, R. Rüger, P. R. T. Schipper, H. van Schoot, G. Schreckenbach, J. S. Seldenthuis, M. Seth, J. G. Snijders, M. Solà, M. Swart, D. Swerhone, G. te Velde, P. Vernooijs, L. Versluis, L. Visscher, O. Visser, F. Wang, T. A. Wesolowski, E. M. van Wezenbeek, G. Wiesenekker, S. K. Wolff, T. K. Woo and A. L. Yakovlev, *ADF2016, SCM, Theoretical Chemistry, Vrije Universiteit, Amsterdam, The Netherlands*, 2016.

[6] G. te Velde and E.J. Baerends, *Phys. Rev. B*, 1991, **44**, 7888.

[7] G. Wiesenekker and E.J. Baerends, *J. Phys. Condens. Matter*, 1991, **3**, 6721.

[8] R. F. Bader, *Atoms in Molecules: A Quantum Theory*, Clarendon Press: Oxford, UK, 1990.

[9] *The Quantum Theory of Atoms in Molecules: From Solid State to DNA and Drug Design*, ed. C. F. Matta and R. J. Boyd, Wiley-VCH Verlag GmbH & Co. KGaA: Weinheim, 2007.

[10] J. P. Perdew, K. Burke and M. Ernzerhof, *Phys. Rev. Lett.*, 1996, **77**, 3865–3868.

[11] V. L. Moruzzi, J. F. Janak and A. R. Williams, *Calculated electronic properties of metals*, Elsevier, 1978.